https://doi.org/10.5194/hess-2020-548
Preprint. Discussion started: 14 December 2020

Hydrology and Earth System Sciences
Discussions

Low and contrasting impacts of vegetation CO_2 fertilization on terrestrial runoff over the past three decades: Accounting for above- and below-ground vegetation-CO_2 effects

Yuting Yang[1], Tim R. McVicar[2,3], Dawen Yang[1], Yongqiang Zhang[4], Shilong Piao[5], Shushi Peng[5], Hylke E. Beck[6]

[1] State Key Laboratory of Hydroscience and Engineering, Department of Hydraulic Engineering, Tsinghua University, Beijing, China

[2] CSIRO Land and Water, Black Mountain, Canberra, ACT 2601, Australia

[3] Australian Research Council Centre of Excellence for Climate Extremes, The Australian National University, Canberra, Australia

[4] Key Laboratory of Water Cycle and Related Land Surface Processes, Institute of Geographic Sciences and Natural Resources Research, Chinese Academy of Sciences, Beijing, China

[5] Sino-French Institute for Earth System Science, College of Urban and Environmental Sciences, Peking University, Beijing 100871, China.

[6] Department of Civil and Environmental Engineering, Princeton University, Princeton, New Jersey, USA

Correspondence to: Yuting Yang (yuting_yang@tsinghua.edu.cn)

https://doi.org/10.5194/hess-2020-548
Preprint. Discussion started: 14 December 2020


Hydrology and Earth System Sciences
Discussions

Abstract. Elevation in atmospheric carbon dioxide concentration (eCO_2) affects vegetation water use, with consequent impacts on terrestrial runoff (Q). However, the sign and magnitude of the eCO_2 effect on Q is still contentious. This is partly due to the poor understanding of the opposing eCO_2-induced water effects at different scales, being water-saving caused by partial stomatal closure at the leaf-level contrasting with increased water-consumption due to increase foliage cover at the canopy level, leading to highly debated findings among existing studies. None of the existing studies implicitly account for eCO_2-induced changes to below-ground vegetation functioning. Here we develop an analytical eco-hydrological framework that includes the effects of eCO_2 on plant leaf, canopy density, and rooting characteristics to attribute changes in Q and detect the eCO_2 signal on Q over the past three decades. Globally, we detect a very small decrease of Q induced by eCO_2 during 1982-2010 (-1.69%). When assessed locally, along the resource availability (α) gradient, a positive trend (p<0.01) in the Q-eCO_2 response is found ranging from a negative response (i.e., eCO_2 reduces Q) in low α regions (typically dry) to a positive response (i.e., eCO_2 increases Q) in high α areas (typically warm and humid). Our findings suggest a minor role of eCO_2 on changes in global Q over the past three decades, yet highlights the negative Q-eCO_2 response in semi-arid and arid regions which may further reduce the limited water resource there.

1 Introduction

Runoff (Q) is the flow of water over the Earth's surface, forming streamflow, becoming one of the most important water resources for irrigation, hydropower and other human needs (Oki and Kanae, 2006). Anthropogenic climate change is expected to alter the global hydrological cycle, with greenhouse gas-induced climate warming intensifying the hydrological cycle (Huntington, 2006). Besides climate, terrestrial vegetation also affects the water cycle. It is well-documented that elevated atmospheric CO_2 concentration (eCO_2) reduces stomatal opening, which in turn suppresses leaf-level transpiration (Field et al., 1995; Donohue et al., 2013). If this were the only mechanism that eCO_2 changed vegetation this would increase runoff (Q) (Gedney et al., 2006). However, eCO_2 increases vegetation foliage cover (Donohue et al., 2013; Zhu et al., 2016), leading to enhanced canopy-level transpiration and consequently reductions of Q (Piao et al., 2007). The two opposite responses of vegetation water use to

https://doi.org/10.5194/hess-2020-548
Preprint. Discussion started: 14 December 2020


Hydrology and Earth System Sciences
Discussions

eCO_2 complicate the net effect of eCO_2 on Q, and existing modeling results are highly debated since they focus on different aspects of how eCO_2 affects the plants and thus the water cycle (Gedney et al., 2006; Piao et al., 2007; Huntington, 2008; Cheng et al., 2014; Yang et al., 2016a; Ukkola et al., 2016). Moreover, those previous modelling results have not been thoroughly validated against observations.

In addition to stomatal and above-ground vegetation structure responding to eCO_2, the below-ground vegetation structure (i.e., rooting depth) is also affected by eCO_2, with eCO_2 increases rooting depth overwhelmingly found in observations (Nie et al., 2013) (Supplementary Tables S1 and S2). Deeper rooting depth means larger plant-available water storage capacity by allowing plants to access deeper soil moisture, which potentially increases transpiration water loss and reduces Q, especially during dry spells (Trancoso et al., 2017; Yang et al., 2016b). To date, no previous eCO_2-Q modeling attempts have explicitly considered the below-ground eCO_2-induced feedback (with the above-ground feedbacks): this paper fills that niche.

Here we use a parsimonious, analytical eco-hydrological model based on the Budyko framework (i.e., the Budyko-Choudury-Porporto, BCP model; Donohue et al., 2012), in combination with an analytical rooting depth model based on ecosystem optimality theory (Guswa, 2008), an analytical CO_2 fertilization model for steady-state vegetation (Donohue et al., 2017) and observed plant stomatal response to eCO_2 (Ainsworth and Rogers, 2007), to detect the impact of eCO_2 on Q changes (dQ) over the past three decades (i.e., 1982-2010). The Budyko framework describes the steady-state (i.e., mean annual scale) hydrological partitioning as a functional balance between atmospheric water supply (i.e., precipitation, P) and demand (i.e., potential evapotranspiration, E_P) and a model parameter that modifies the climate-hydrology relationship (Choudhury, 1999; Donohue et al., 2012). In this framework, both E_P and the land surface parameter are affected by the response of vegetation to eCO_2 (see Methods). The developed framework allows analytical and transparent attribution of dQ changes, which overcomes the uncertainty raised from non-linear interactions among numerous processes when attributing dQ numerically by using bottom-up earth system models (Yang et al., 2015). To examine the long-term eCO_2 impact and to minimize year-to-year "transient" effects (i.e., water storage changes), we performed our analyses using sequential 5-year periods (Yang et al., 2016a; Han et al., 2020), resulting

https://doi.org/10.5194/hess-2020-548
Preprint. Discussion started: 14 December 2020


Hydrology and Earth System Sciences
Discussions

in six 5-year-means during 1982-2010, with the first period containing 4 years. Additionally, since vegetation response to eCO_2 can be greatly mediated by the availability of other resources (e.g., water, light and nutrients) (Donohue et al., 2013; Donohue et al., 2017; Nenami et al., 2003; Yang et al., 2016a; Norby et al., 2010), we examine the impact of eCO2 on *Q* along a resource availability gradient (Donohue et al., 2017; Friedkubgstein et al., 1999) (see Methods). The resource availability is typically low in dry environments and increases as the climate becomes more humid, which enable us to detect the signal of eCO_2 on *Q* across a dry – wet gradient.

2 Material and methods

2.1 Runoff simulation

The Budyko-Choudhury-Porporato (BCP) model was adopted here to simulate *Q* and to attribute changes in *Q* (Yang et al., 2016b; Donohue et al., 2012). Choudhury's formulation of the Budyko curve is (Choudhury, 1999):

$$E = \frac{PE_{\mathrm{P}}}{(P^n + E_{\mathrm{P}}{}^n)^{1/n}} \quad (1)$$

where *E* is the actual evapotranspiration (mm yr^{-1}). *P* is the precipitation depth (mm yr^{-1}). E_P is the potential evapotranspiration (mm yr^{-1}) and is estimated here using the Shuttleworth-Wallace two-source evapotranspiration model (Shuttleworth and Wallace, 1985) with the assumption of full soil moisture supply (by taking soil surface resistance equal to zero and stomatal resistance equal to its non-water-stressed value) while allowing leaf area and leaf-level conductance to vary with atmospheric CO_2 concentration (C_a) (Milly and Dunne, 2016). A recent study by Milly and Dunne (2016) showed that the Shuttleworth-Wallace model could most satisfactorily reproduce E_P estimates from climate models under eCO_2. *n* is a unitless model parameter that encodes all factors other than mean climate conditions and modifies the partitioning of *P* between *E* and *Q*. For steady-state conditions, *Q* is calculated by subtracting *E* from *P* as a result of catchment water balance.

The probabilistic steady state solution of Porporato's stochastic dynamic soil moisture model shares a similar form with the Budyko curve (Porporato et al., 2004). Porporato's parameter ω is a

https://doi.org/10.5194/hess-2020-548
Preprint. Discussion started: 14 December 2020


Hydrology and Earth System Sciences
Discussions

dimensionless parameter, which is a function of effective rooting depth (Z_e, mm), mean rainfall intensity (β, mm per event) and soil water holding capacity (θ, $mm^3\ mm^{-3}$) and exhibits a close relationship with the Choudhury's parameter *n* (Yang et al., 2016b; Porporato et al., 2004). Taking data from Porporato et al. (2004), we deduced the relationship between *n* and ω as (R^2=0.96, p<0.001; Supplementary Figure S1):

$$n = 0.82\ln(\omega) + 0.636 = 0.82\ln(\frac{Z_e\theta}{\beta}) + 0.636 \quad (2)$$

Effective rooting depth (Z_e) was determined using an analytical carbon cost-benefit model based on ecosystem optimality theory proposed by Guswa (2008). The Z_e model is given as (Guswa, 2008):

$$Z_e = \frac{\beta}{\theta(1-W)}\ln(X) \quad (3)$$

$$X = \begin{cases} W\left[1+\frac{\theta}{\beta}\frac{(1-W)^2}{2A} - \sqrt{\frac{\theta}{\beta}\frac{(1-W)^2}{A} + (\frac{\theta}{\beta}\frac{(1-W)^2}{2A})^2}\right] & \text{if} \quad W>1 \\ W\left[1+\frac{\theta}{\beta}\frac{(1-W)^2}{2A} + \sqrt{\frac{\theta}{\beta}\frac{(1-W)^2}{A} + (\frac{\theta}{\beta}\frac{(1-W)^2}{2A})^2}\right] & \text{if} \quad W<1 \end{cases} \quad (4)$$

$$A = \frac{\gamma_r \times RLD}{SRL \times WUE} \times \frac{1}{E_{P\_T} \times f_{GS}} \quad (5)$$

where *W* is the ratio of mean annual *P* over potential transpiration, E_{P_T}. γ_r is the root respiration rate (g C g^{-1} roots day^{-1}), which is quantified using the Q_{10} equation (Lloyd and Taylor, 1994). *RLD* is the root length density (cm roots cm^{-3} soil) and *SRL* is the specific root length (cm roots g^{-1} roots). We fixed *RLD* to be 0.1 cm roots cm^{-3} soil and *SRL* to be 1500 cm roots g^{-1}, representing the median value of these two parameters reported in the literature, respectively (Caldwell, 1994; Eissenstat, 1997; Fitter and Hay, 2002; Pregitzer et al., 2002). f_{GS} is the fraction of growing season within a year, with the growing season length quantified according to Zhu et al. (2016). *WUE* is the photosynthetic water use efficiency (g C cm^{-3} H_2O), which is determined for the first period (i.e., 1982-1985) from the ensemble means from eight Earth system models (described later) of annual gross primary production (*GPP*) and E_T estimates (*i.e.*, $WUE=GPP/E_T$). For the following periods, *WUE* was estimated by considering the

https://doi.org/10.5194/hess-2020-548
Preprint. Discussion started: 14 December 2020


Hydrology and Earth System Sciences
Discussions

effects of changes in C_a and vapor pressure deficit (v) on *WUE* (Donohue et al., 2013; Wong et al., 1979; Farquhar et al., 1993):

$$WUE_{t+1} = WUE_t + WUE_t\left(\frac{C_{a,t+1} - C_{a,t}}{C_{a,t}} - \frac{1}{2}\frac{v_{t+1} - v_t}{v_t}\right) \quad (6)$$

where t is time in year. Note that the above equation implicitly assumes the same upscaling factor when converting the leaf-level assimilation and transpiration to the canopy level for a given location (Donohue et al., 2017). The spatial pattern of mean annual Z_e is shown in Supplementary Figure S2.

2.2 Attribution runoff changes

We used the BCP model to attribute changes in Q (dQ) due to different influencing factors following the method developed by Roderick and Farquhar (2011). To first order, change in Q (dQ) is:

$$dQ = \frac{\partial Q}{\partial P}dP + \frac{\partial Q}{\partial E_P}dE_P + \frac{\partial Q}{\partial n}dn \quad (7)$$

where $\partial Q/\partial P$, $\partial Q/\partial E_P$ and $\partial Q/\partial n$ represent the sensitivity of Q to changes in P, E_p and n, respectively, and can be expressed as:

$$\frac{\partial Q}{\partial P} = 1 - \frac{E}{P}\left(\frac{{E_P}^n}{P^n + {E_P}^n}\right) \quad (8)$$

$$\frac{\partial Q}{\partial E_P} = -\frac{E}{E_P}\left(\frac{P^n}{P^n + {E_P}^n}\right) \quad (9)$$

$$\frac{\partial Q}{\partial n} = -\frac{E}{n}\left[\frac{\ln(P^n + {E_P}^n)}{n} - \frac{P^n \ln P + {E_P}^n \ln E_P}{P^n + {E_P}^n}\right] \quad (10)$$

The physiological (stomatal conductance, C_s) and structural (Leaf area index, L, and effective rooting depth, Z_e) impact both E_P and n. More specifically, decreases in C_s lower the transpiration rate per leaf area, whereas increases in L and Z_e enhance the canopy level transpiration rate. Additionally, increases in L also reduce soil evaporation by shading the soil surface (Shuttleworth and Wallace, 1985). The impact of eCO_2 on parameter n is expressed through its impact on Z_e. On one hand, increases in *WUE* induced by eCO_2 permit a larger vegetation carbon uptake per amount of water loss, potentially leading

https://doi.org/10.5194/hess-2020-548
Preprint. Discussion started: 14 December 2020


Hydrology and Earth System Sciences
Discussions

to more carbon allocated to roots and thus a deeper Z_e. Conversely, increases in plant water demand (as quantified by potential transpiration) would require plants to develop a deeper root to access to soil moisture at deeper depths, and *vice versa* (Guswa, 2008). As a result, we write E_P and Z_e as:

$$E_P = f(C_a, E_{P\_M}) \tag{11}$$

$$Z_e = g(C_a, O) \tag{12}$$

and changes in E_P and Z_e are given by:

$$dE_P = \frac{\partial E_P}{\partial C_a} dC_a + \frac{\partial E_P}{\partial E_{P\_M}} dE_{P\_M} \tag{13}$$

$$dZ_e = \frac{\partial Z_e}{\partial C_a} dC_a + \frac{\partial Z_e}{\partial O} dO \tag{14}$$

where E_{P_M} is the meteorological component of E_P (without considering C_a). O represents factors other than eCO_2 that affects Z_e, which effectively encodes the climate change-induced vegetation change.

Combining Eqs. (2), (7), (13) and (14), we have:

$$dQ = \frac{\partial Q}{\partial P} dP + \left(\frac{\partial Q}{\partial E_P} \frac{\partial E_P}{\partial C_a} + \frac{0.82}{Z_e} \frac{\partial Q}{\partial n} \frac{\partial Z_e}{\partial C_a} \right) dC_a + \frac{\partial Q}{\partial E_P} \frac{\partial E_P}{\partial E_{P\_M}} dE_{P\_M} + \frac{0.82}{\beta} \frac{\partial Q}{\partial n} d\beta + \frac{0.82}{Z_e} \frac{\partial Q}{\partial n} \frac{\partial Z_e}{\partial O} O \tag{15}$$

The first term on the right hand of Eq. (15) represents dQ caused by P change, the second term represents dQ caused by eCO_2 and the third term calculates dQ induced by changes in E_{P_M}. To maintain simplicity, we calculate E_{P_M}-induced dQ by subtracting the effect of eCO_2-caused changes in E_P on Q from dQ caused by changes in E_P (i.e., $\frac{\partial Q}{\partial E_P} dE_P - \frac{\partial Q}{\partial E_P} \frac{\partial E_P}{\partial C_a} dC_a$). The fourth and fifth terms on the right hand of Eq. (15) represent dQ caused by changes in rainfall intensity and climate change-induced vegetation change, respectively, and we group them as one factor in the attribution of dQ (i.e., other factors in Fig. 3). Since our primary focus was to examine how eCO_2 affect Q and its relative

https://doi.org/10.5194/hess-2020-548
Preprint. Discussion started: 14 December 2020


Hydrology and Earth System Sciences
Discussions

importance to changes in P and E_P the other factors driving dQ change were estimated as the residual of Eq. (15). By introducing Eqs. (9) and (10) into Eq. (15), the sensitivity of Q to eCO_2 ($S_{Q\_to\_eCO2}$) is written as,

$$S_{Q\_to\_eCO2} = -\frac{E}{E_P}\left(\frac{P^n}{P^n + E_P{}^n}\right)\frac{\partial E_P}{\partial C_a} - \frac{E}{n}\frac{0.82}{Z_e}\left[\frac{\ln(P^n + E_P{}^n)}{n} - \frac{P^n \ln P + E_P{}^n \ln E_P}{P^n + E_P{}^n}\right]\frac{\partial Z_e}{\partial C_a} \quad (16)$$

The sensitivities of E_P and Z_e to eCO_2 (i.e., $\frac{\partial E_P}{\partial C_a}$ and $\frac{\partial Z_e}{\partial C_a}$) are quantified by numerically running the E_P model and Z_e model with and without changes in C_a, respectively. The difference between the two simulations under the two C_a scenarios is considered the net effect of eCO_2.

2.3 Stomatal conductance response to eCO_2

The response of leaf-level stomatal conductance (C_s) response to eCO_2 was determined using 244 field observations across a broad range of bioclimates (Ainsworth and Rogers, 2007). We linearly rescaled the reported change in C_s for the magnitude of eCO_2 in each study to obtain the sensitivity of C_s to eCO_2: that is, the percentage change in C_s per 1% increase in C_a. We then classified the 244 observations based on their biome type to construct a biome type-based look-up table of C_s sensitivity to eCO_2.

2.4 Resource availability index and leaf area index response to eCO_2

The response of L to eCO_2 was predicted based on the response of WUE to eCO_2 adjusted by the local resource availability. We define the site resource availability index (α) based on growing season mean L following Donohue et al. (2017). This is because that observed L at a site is the net response to the local growing conditions and provides an effective proxy of the growing conditions experienced by plants (Donohue et al., 2017). Another advantage of this approach is that L can be readily measured directly or remotely. We calculated α as,

$$\alpha = 1 - e^{-\tau L} \quad (17)$$

https://doi.org/10.5194/hess-2020-548
Preprint. Discussion started: 14 December 2020


Hydrology and Earth System Sciences
Discussions

where τ is an exponential extinction coefficient, which typically varies from 0.3 to 1.2 (Campbell and Norman, 1998) and is set to be 0.7 herein. Broadly across the globe, α also corresponds well with climate aridity. The calculated α increases from 0.0 with low resource availability (typically dry) to 1.0 with high resource availability (typically warm and humid) (Figure 1). This suggests a predominant role of the climate in shaping the global vegetation pattern (Nemani et al., 2003). This also implies that the resource limitations on plant growth are mainly exerted by climate, consistent with the framework of climate limitation on vegetation proposed in previous studies (Nemani et al., 2003; Budyko, 1974; Yang et al., 2015). Then following Norby and Zak (2011), who showed that the observed response of L to eCO_2 was a non-linear function of L, we estimated the relative change in L induced by eCO_2 per Donohue et al., (2017):

$$\frac{dL}{L}=\frac{dWUE}{WUE}(1-\alpha)^2=(\frac{dC_a}{C_a}-\frac{1}{2}\frac{dv}{v})e^{-2\tau L} \quad (18)$$

2.5 Data

To focus on the impacts of eCO_2 on Q via feedbacks through vegetation and to eliminate potential human impacts on Q, we limit our analyses to 2,268 strictly selected unimpaired catchments located across the globe (Figure 2). Originally, daily and/or monthly Q observations were collected from more than 22,000 catchments globally (Beck et al., 2019). Three selection criteria were implemented to ensure that only catchments with a continuous Q records that are negligibly affected by human were used. First, catchments with >5% missing data during the entire study period (1982-2010) were removed. A linear interpolation was applied to fill the gaps in the remaining daily Q series. Second, catchments smaller than 100 km^2 were excluded. This is to ensure that at least one precipitation pixel (i.e., 0.1° × 0.1°, or ~100 km^2) is included for a catchment. Third, we excluded catchments where observed Q is likely to be affected by human interventions, including catchments with: (i) significant forest gain or loss (> 2% of the total catchment area) (Hansen et al., 2013); (ii) irrigated areas larger than 2% (Siebert et al., 2005); (iii) urban areas (http://ionia.esrin.esa.int) larger than 2%; and (iv) the presence of large dams (Lehner et al., 2011) (i.e., where the reservoir capacity in a catchment is larger

https://doi.org/10.5194/hess-2020-548
Preprint. Discussion started: 14 December 2020


Hydrology and Earth System Sciences
Discussions

than 10% of the catchment mean annual Q). Exactly 2,268 catchments pass the above selection criteria (Figure 2).

Precipitation from 1981 through 2010 was taken from the Multi-Source Weighted-Ensemble Precipitation (MSWEP) version 2 dataset, which has a three-hour temporal resolution and 0.1° spatial resolution (Beck et al., 2019). Other climate variables, including net radiation, air temperature, relative humidity, air pressure and wind speed were generated during MsTMIP (Wei et al., 2014). Monthly C_a from 1982-2010 was obtained from the Hawaiian Mauna Loa Observatory (http://www.esrl.noaa.gov/gmd/obop/mlo/) and we assume a uniform C_a concentration across the globe at the mean annual scale (i.e., five years). Monthly L for 1982-2010 was derived from Zhu et al. (2013) based on AVHRR GIMMS-3g NDVI data (Pinzon and Tucker, 2014). Land cover classification was acquired from the Moderate Resolution Imaging Spectroradiometer (MODIS) land use map (MOD12Q1) available from the NASA data center (Friedl et al., 2010). The global C4 vegetation fraction was obtained from the NASA data center (http://webmap.ornl.gov/ogcdown/dataset.jsp?ds_id=932). Soil texture data at 30'' spatial resolution was acquired from the Harmonized World Soil Database (HWSD) (Nachtergaele, 2009), which was used to determine the value of θ according to the US Department of Agriculture (USDA) soil classification (Saxton and Rawls, 2006). These gridded data were further aggregated for individual catchments at a mean annual scale (i.e., five years).

3 Results and discussion

3.1 Validation of the BCP model in runoff estimation

The validity of the BCP model is tested by comparing the estimated Q with observed Q, in terms of both spatial and temporal variability, at the 2,268 unimpaired catchments (Figure 3). Spatially, the BCP model well captures the observed spatial variability in Q at the mean annual scale, with a coefficient of determination (R^2) of 0.93, root-mean-squared error (RMSE) of 87.9 mm yr^{-1} and mean bias (estimated Q minus observed Q) of -11.4 mm yr^{-1} (Figure 3a) Temporally, trends in mean annual Q are also reasonably reproduced by the BCP model, which produces an R^2 of 0.71, RMSE of 0.71 mm yr^{-2} and

https://doi.org/10.5194/hess-2020-548
Preprint. Discussion started: 14 December 2020


Hydrology and Earth System Sciences
Discussions

mean bias of -0.05 mm yr^{-2} (Figure 3b) In addition, we also perform a sensitivity analysis by comparing the simulated Q using the BCP model with and without considering eCO_2. Results show that the BCP model, when considering eCO_2, performed differentially better in estimating Q trends than the BCP model without considering eCO_2, suggesting that the developed analytical framework herein can well capture the eCO_2 signal on the observed Q changes (Figure 3d).

3.2 Plant physiological and structural responses to eCO_2

The physiological response of plant to eCO_2, that is, the response of stomatal conductance (C_s) to eCO_2 is directly compiled from field experiments and summarized for each plant functional type in Ainsworth and Rogers (2007) (also see Supplementary Figure S3). All those field experiments report a reduction of C_s in response to eCO_2, with the largest (lowest) C_s reduction found in C4 crops (shrubs) for the same level of eCO_2. On average, for a 1% increase in atmospheric CO_2 concentration (C_a), C_s decreases by 0.47% ± 0.12% (mean ± one standard deviation), which means that C_s decreases by 5.67% ± 1.47% under a 12.1% increase in C_a over 1982-2010 (i.e., from ~343.7 ppm in 1982-1985 to 385.2 ppm in 2006-2010; Keeling et al., 2011). This result is consistent with a recent isotope-based study (i.e., ~5% reduction of C_s during the past three decades, Frank et al. 2015).

For structural response, averaged across global vegetated lands, elevated C_a has caused an increase of L by 2.1% over the past three decades (Figure 4a and b). Despite this relatively small fertilization effect of eCO_2 on L at the global scale, an evident gradient is found in the L - eCO_2 response that a larger eCO_2-induced relative L increase is found in low resource availability regions (smaller α value in Figure 1a), and *vice versa* (Figure 4b). This modelled pattern of L - eCO_2 response agrees very well observations at the Free-Air CO_2 Enrichment (FACE) observations (R^2=0.96, p<0.01; Figure 4c) and is also consistent with large-scale satellite-based observations (Donohue et al., 2013; Zhu et al., 2016; Yang et al., 2016a).

In terms of Z_e, elevated C_a over the past three decades has resulted in a very minor (~1%) overall increase of Z_e averaged across the globe (Figure 4e). Since large-scale observations of Z_e in response to eCO_2 are not available, we are not able to quantitatively validate the estimated response of Z_e to eCO_2.

https://doi.org/10.5194/hess-2020-548
Preprint. Discussion started: 14 December 2020


Hydrology and Earth System Sciences
Discussions

Nevertheless, the modelled result that eCO_2 increases Z_e is overwhelmingly found in site- and/or plant-level observations (Nie et al., 2013) (Supplementary Tables S1 and S2). Moreover, similar with L, the response of Z_e to eCO_2 also exhibits a notable difference along the resource availability gradient (Figure 4d and 4e). The positive response of Z_e to eCO_2 is larger in low α regions and gradually decreases as the resource availability becomes higher. In high α regions (e.g., tropical rainforest and southeast Asia), Z_e even shows a slightly decreases in response to eCO_2, suggesting a reduced plant water need in a high C_a atmosphere in those regions.

3.3 Attribution of runoff changes over 1982-2010

During the last three decades, atmospheric CO_2 concentration (C_a) increased by ~12.1%. For the same period, the BCP model detected a very small reduction in Q of ~0.73% (or 2.8 mm yr^{-1}) induced by eCO_2 across the 2,268 studied catchments (Figure 5). The overall negative effect of eCO_2 on Q suggests that the structural forcing of eCO_2 on vegetation water consumption (both above- and below-ground) outweighs the physiological effect of eCO_2 driving leaf-level water saving. Despite the overall small effect averaged across all catchments, a significant positive trend (p<0.01) in the Q-eCO_2 response is found along the resource availability gradient, from a negative response in low α catchments to a positive response in high α catchments (Figure 5).

We then attribute dQ to different factors between 1982-1985 and 2006-2010 for the study catchments (Figure 6). Compared with the early 1980s, mean observed Q over the 2,268 catchments in the late 2010s decreased by ~5.8 mm yr^{-1}, and the observed pattern with comparable magnitude in dQ is well captured by the BCP model (Figure 6). The impact of eCO_2 on dQ is estimated to be -2.3 mm yr^{-1} averaged over all 2,268 catchments. Consistent with relative Q changes (in %; Figure 5), the impacts eCO_2 on the absolute Q change (in mm yr^{-1}) also exhibit significant upward trend as α increases (~0.97 mm yr^{-1} per 0.1 increase in α, p<0.01). Compared to that, decreases in P led to a 2.7 mm yr^{-1} decreases in Q, and enhanced E_P has resulted in a decreased Q by 1.6 mm yr^{-1} (Figure 6a). The comparable magnitudes of dQ induced by dP and eCO_2 only exist when averaged across all 2,268 catchments, while for each resource availability category, the impact of P on Q generally dominates dQ and is often much higher than that of eCO_2 (Figure 7). As for the impact E_P on Q, it also shows a notable gradient with

https://doi.org/10.5194/hess-2020-548
Preprint. Discussion started: 14 December 2020


Hydrology and Earth System Sciences
Discussions

changes in α as detected for the eCO_2 effect, with the impact of E_P on Q being increasingly negative as α raises (Figure 6b-f). Other factors include changes in rainfall intensity (Porporato et al., 2004) and climate change-induced vegetation change (e.g., higher L) have, in general, exerted a small negative impact on Q.

The same conclusions that the impacts of eCO_2 on vegetation have limited yet contrasting (between warm-humid, high α regions and dry, low α regions) feedbacks on Q retain beyond the 2,268 catchments (Figure 7a and b). At the global scale, an increase in C_a by 1% only leads to a decrease of Q by ~0.14% (equivalent to ~1.69% for the range of eCO_2 experienced over the past three decades). This 1.69% reduction in Q, under the context of 12.1% increases in C_a, demonstrates a muted response of Q to eCO_2. The sensitivity of Q to eCO_2 ($S_{Q\_to\_eCO2}$) is generally more negative in global arid ecosystems where α is low, with an exception in extreme arid zones (i.e., when α<0.1; Figures 7a and b). This is because in extremely dry areas, the availability of water defines the outcome and the sensitivity of Q to any changes in land surface properties is very small (Donohue et al., 2013; Roderick et al., 2014). The negative $S_{Q\_to\_eCO2}$ diminishes quickly as α increases and turns to be a positive $S_{Q\_to\_eCO2}$ in high α regions. The overall small $S_{Q\_to\_eCO2}$ is further manifested when comparing $S_{Q\_to\_eCO2}$ with the sensitivities of Q to climate variables (i.e., P and E_P). Averaged over the globe, a same relative change in P and E_P would respectively lead to a ~10-times and ~4-times stronger impact on Q than eCO_2 does, highlighting a predominant role of climate in shaping the global Q regime (Figure 7c-f and Supplementary Figure S4).

4. Discussion and concluding remarks

Elevation in atmospheric CO_2 concentration is regarded as the ultimate driver of anthropogenic climate change, with consequent impacts on terrestrial runoff. Although the impacts of climate change on Q has been extensively documented in previous studies, the response of Q to eCO_2 through vegetation feedbacks is less understood and remains controversial in existing studies (Gedney et al., 2006; Piao et al., 2007; Huntington, 2008; Cheng et al., 2014; Yang et al., 2016a; Ukkola et al., 2016). Here, by developing an analytical attribution framework, we detected a very small response of global Q to eCO_2-induced changes in vegetation functioning (Figure 5-7), suggesting that the eCO_2 vegetation feedback

https://doi.org/10.5194/hess-2020-548
Preprint. Discussion started: 14 December 2020


Hydrology and Earth System Sciences
Discussions

only exert a minor impact on water resources for the range of eCO_2 that we have experienced over the past three decades.

We also detected a significant positive trend (p<0.01) in the Q-eCO_2 response along the resource availability gradient (Figure 5-7), which is consistent with field experiments (Norby and Zak, 2011; De Kauwe et al., 2013; Körner and Arnone, 1992) (Figure 4c), satellite observations (Donohue et al., 2013; Zhu et al., 2016; Yang et al., 2016a), and model attributions (Cheng et al., 2014; Lian et al., 2018). This Q-eCO_2 response mechanism suggests that the structural response of vegetation to eCO_2 (i.e., increases in L and Z_e) is larger in areas with lower resource availability, and gradually decreases as resources become less limiting on plant growth (Figure 4). The positive response of Q to eCO_2 in high α catchments (primarily located in tropical rainforests) implies a dominant effect of eCO_2-induced partial stomatal closure over increases in L and Z_e on E in these environments. This is reasonable, as both theoretical predictions and *in-situ* observations have consistently reported a negligible response of L to eCO_2 in humid and close-canopy environments (Donohue et al., 2017; Yang et al., 2016a; Norby and Zak, 2011; Körner and Arnone, 1992). In such environments, water is generally abundant with light and/or nutrient availability being the most limiting resources for vegetation growth (Nemani et al., 2003; Yang et al., 2015), and plants have evolved to efficiently capture light by maximizing their above-ground structure (i.e., L). As a result, in these tropical rainforests plants have already absorbed most of the incident light and any extra leaves would not materially increase the light absorption (Yang et al., 2016a).

Our findings have important implications for improved understanding of the global hydrological cycle and managing the world's water resources in a changing climate. Climate models have predicted an increased Q that is primarily driven by an increased P for the 21st century (Milly and Dunne, 2016; Swann et al., 2016; Yang et al., 2018). Here we show that eCO_2 would mitigate this positive impact of climate change on Q in relatively dry regions but exaggerate the Q increase in relatively wet regions via its impacts on vegetation water use. In addition, higher C_a and increased P enhance the availability of resource for vegetation growth, which increases vegetation coverage or L (Piao et al., 2020; Zhang et al., 2020a; Zhang et al., 2020b). This suggests that the structural response of vegetation to eCO_2 may

https://doi.org/10.5194/hess-2020-548
Preprint. Discussion started: 14 December 2020

eventually decrease and the physiological effect of vegetation to eCO_2 may become increasingly dominant in the overall response of vegetation water use to eCO_2, leading to an increasing water-saving effect of plant in response to eCO_2 under future climate change (Zhang et al., 2020b). In fact, analyses of the state-of-the-art climate model outputs have already consistently shown this water-saving effect of eCO_2 at the global scale and especially in relatively warm and humid environments where L is high (Yang et al., 2019). Yet, the impacts of eCO_2 on Q in relatively dry regions are still highly uncertain and show a great diversity between climate models (Zhang et al., 2020b). In this light, our findings based on the well-validated analytical framework provide insightful guidance for climate model development that improves the models' capability in representing the vegetation and hydrological responses to eCO_2.

Data availability

All data for this paper are properly cited and referred to in the reference list.

Author contribution

YY and TRM designed the study. YY performed the calculation and drafted the manuscript. TRM, DY, YZ, SP, SP, and HEB contributed to results discussion and manuscript writing.

Competing interests

The authors declare that they have no conflict of interest.

Acknowledgements

This study was supported by the National Natural Science Foundation of China (Grant No. 42071029), the Qinghai Department of Science and Technology (Grant No. 2019-SF-A4), the Ministry of Science and Technology of China (Grant No. 2019YFC1510604), and the Guoqiang Institute of Tsinghua University (Grant No. 2019GQG1020) T. McVicar acknowledges support from CSIRO Land and Water. The following organizations are thanked for providing observed streamflow data: the United

https://doi.org/10.5194/hess-2020-548
Preprint. Discussion started: 14 December 2020

Hydrology and Earth System Sciences
Discussions

States Geological Survey (USGS), the Global Runoff Data Centre (GRDC), the Brazilian Brazilian Agência Nacional de Águas, the Water Survey of Canada (WSC), the Australian Bureau of Meteorology (BoM), and the Chilean Chilean Center for Climate and Resilience Research (CR2).

References

Ainsworth, A. E., and Rogers, A.: The response of photosynthesis and stomatal conductance to rising [CO_2]: mechanisms and environmental interactions, Plant Cell Environ., 30, 258-270, https://doi.org/10.1111/j.1365-3040.2007.01641.x, 2007.

Beck, H. E. et al.: MSWEP V2 global 3-hourly 0.1° precipitation: methodology and quantitative assessment. Bulletin of the American Meteorological Society., 3, 473-500, https://doi.org/10.1175/BAMS-D-17-0138.1, 2019.

Beck H.E., et al.: Bias Correction of Global High-Resolution Precipitation Climatologies Using Streamflow Observations from 9372 Catchments. Journal of Climate, 33, 1299-1315, 2020.

Beck, H. E., Wood, E. F., Pan, M., Fisher, C. K., Miralles, D. G., Van Dijk, A.I.J.M., McVicar, T. R., and Adler, R. F.: MSWEP V2 global 3-hourly 0.1° precipitation: methodology and quantitative assessment, Bulletin of the American Meteorological Society, 100(103), 473-500, 2019. https://doi.org/10.1175/BAMS-D-17-0138.1

Budyko, M. I.: Climate and life. Academic, New York, 1974.

Caldwell, M. M.: in Exploitation of Environmental Heterogeneity by Plants (ed Caldwell M. M.) 325-347. Academic, San Diego, 1994.

Campbell, G. S., and Norman, J. M.: An Introduction to Environmental Biophysics. Springer, New York, 1998.

Cheng, L., Zhang, L., Wang, Y. P., Yu, Q., Eamus, D., and O'Grady, A.: Impacts of elevated CO_2, climate change and their interactions on water budgets in four different catchments in Australia. J. Hydrol., 519, 1350-1361, https://doi.org/10.1016/j.jhydrol.2014.09.020, 2014.

Choudhury, B.: Evaluation of an empirical equation for annual evaporation using field observations and results from a biophysical model. J Hydrol., 216, 99-110, https://doi.org/10.1016/S0022-1694(98)00293-5, 1999.

De Kauwe, M. G. et al.: Forest water use and water use efficiency at elevated CO_2: a model-data intercomparison at two contrasting temperate forest FACE sites. Glob. Change Biol. 19, 1759-1779, https://doi.org/10.1111/gcb.12164, 2013.

Donohue, R. J., Roderick, M. L., McVicar, T. R., and Farquhar, G. D.: Impact of CO_2 fertilization on maximum foliage cover across the globe's warm, arid environments, Geophys. Res. Lett., 40, 3031-3035, https://doi.org/10.1002/grl.50563, 2013.

Donohue, R. J., Roderick, M. L., McVicar, T. R., and Yang, Y.: A simple hypothesis of how leaf and canopy-level transpiration and assimilation respond to elevated CO_2 reveals distinct response patterns between disturbed and undisturbed vegetation. J. Geophys. Res. Biogeosci., 122, 168-184, https://doi.org/10.1002/2016JG003505, 2017.

Donohue, R. J., Roderick, M. L., and McVicar, T. R.: Roots, storms and soil pores: Incorporating key ecohydrological processes into Budyko's hydrological model. J. Hydrol., 436, 35-50, https://doi.org/10.1016/j.jhydrol.2012.02.033, 2012.

Eissenstat, D. M.: in Ecology in Agriculture (ed L.E. Jackson) 173-199. Academic, New York, 1997.

Falcone, J. A., Carlisle, D. M., Wolock, D. M., and Meador, M. R.: GAGES: A stream gage database for evaluating natural and altered flow conditions in the conterminous United States. Ecology, 91, 621–621, https://doi.org/10.1890/09-0889.1, 2010.

Farquhar, G. D. et al.: Vegetation effects on the isotope composition of oxygen in atmospheric CO_2. Nature, 363, 439-443, 1993.

Field, C. B., Jackson, R. B., and Mooney, H. A.: Stomatal responses to increased CO_2: implications from the plant to the global scale. Plant Cell Environ., 18, 1214-1225, https://doi.org/10.1111/j.1365-3040.1995.tb00630.x, 1995.

Fitter, A. H., and Hay, R. K. M.: Environmental Physiology of Plants. Academic, London, 2002.

Frank, D. C. et al.: Water-use efficiency and transpiration across European forests during the Anthropocene. Nature Clim. Change, 5, 579-583, https://doi.org/10.1038/nclimate2614, 2015.

Friedl, M. A., Sulla-Menashe, D., Tan, B., Schneider, A., Ramankutty, N., Sibley, A., and Huang, X.: MODIS Collection 5 global land cover: Algorithm refinements and characterization of new datasets. Remote Sens. Environ., 114, 168-182, https://doi.org/10.1016/j.rse.2009.08.016, 2010.

Friedlingstein, P., Joel, G., Field, C. B. and Fung, I. Y.: Toward an allocation scheme for global terrestrial carbon models. Glob. Change Biol., 5, 755-770, https://doi.org/10.1046/j.1365-2486.1999.00269.x, 1999.

Gedney, N., Cox, P. M., Betts, R. A., Boucher, O., Huntingford, C., and Stott, P. A.: Detection of a direct carbon dioxide effect in continental river runoff records. Nature, 439, 835-838, https://doi.org/10.1038/nature04504, 2006.

Guswa, A. J.: The influence of climate on root depth: A carbon cost-benefit analysis. Water Resour. Res., 44, WR006384, https://doi.org/10.1029/2007WR006384, 2008.

Han, J. T., Yang, Y., Roderick, M. L., McVicar, T. R., Yang, D. W., Zhang, S. L., and Beck, H. E.: Assessing the steady - state assumption in water balance calculation across global catchments. Water Resour. Res., 56, e2020WR027392, https://doi.org/10.1029/2020WR027392, 2020.

Hansen, M. C. et al.: High-Resolution Global Maps of 21st-Century Forest Cover Change. Science, 342, 850-853, https://doi.org/10.1126/science.1244693, 2013.

Huntington, T. G.: CO_2-induced suppression of transpiration cannot explain increasing runoff. Hydrol. Process., 22, 311-314, https://doi.org/10.1002/hyp.6925, 2008.

Huntington, T. G.: Evidence for intensification of the global water cycle: Review and synthesis. J. Hydrol., 319, 83-95, https://doi.org/10.1016/j.jhydrol.2005.07.003, 2006.

Keeling, C.D. et al.: Exchanges of atmospheric CO_2 and $^{13}CO_2$ with the terrestrial biosphere and oceans from 1978 to 2000. I. Global aspects, SIO Reference Series, No. 01-06, Scripps Institution of Oceanography, San Diego, 88 pages, 2001.

Körner, C., and Arnone, J. A.: Responses to Elevated Carbon Dioxide in Artificial Tropical Ecosystems. Science, 257, 1672-1675, https://doi.org/10.1126/science.257.5077.1672, 1992.

Lehner, B. et al. High-resolution mapping of the world's reservoirs and dams for sustainable river-flow management. Front. Ecol. Environ., 9, 494-502, https://doi.org/10.1890/100125, 2011.

Lian, X., Piao, S., Huntingford, C., Li, Y., Zeng, Z., Wang, X., Ciais, P., McVicar, T., Peng, S., Ottle, C., Yang, H., Yang, Y., Zhang, Y., and Wang, T.: Partitioning global land evapotranspiration using CMIP5 models constrained by observations, Nat. Clim. Change, 8, 640-646, https://doi.org/10.1038/s41558-018-0207-9, 2018.

Lloyd, J., and Taylor, J. A.: On the Temperature Dependence of Soil Respiration. Funct. Ecol., 8, 315-323, https://www.jstor.org/stable/2389824, 1994.

Milly, P. C. D., and Dunne, K. A.: Potential evapotranspiration and continental drying, Nat. Clim. Change, 6, 946-949, https://doi.org/10.1038/nclimate3046, 2016.

Nachtergaele, F., van Velthuizen, H., and Verelst, L.: Harmonized World Soil Database. FAO, Rome Italy and IIASA, Laxenburg Austria, 2009.

Nemani, R., Keeling, C. D., Hashimoto, H., Jolly, W. M., Piper, S. C., Tucker, C. J., Myneni, R. B., and Running, S. W.: Climate-Driven Increases in Global Terrestrial Net Primary Production from 1982 to 1999. Science, 300, 1560-1563, https://doi.org/10.1126/science.1082750, 2003.

Nie, M., Lu, M., Bell, J., Raut, S. and Pendall, E.: Altered root traits due to elevated CO_2: a meta-analysis. Glob. Ecol. Biogeogr., 22, 1095-1105, https://doi.org/10.1111/geb.12062, 2013.

Norby, R. J., Warren, J. M., Iversen, C. M., Medlyn, B. E., and McMurtrie, R. E.: CO_2 enhancement of forest productivity constrained by limited nitrogen availability. Proc. Natl. Acad. Sci., 107, 19368-19373, https://doi.org/10.1073/pnas.1006463107, 2010.

Norby, R. J., and Zak, D. R.: Ecological Lessons from Free-Air CO_2 Enrichment (FACE) Experiments. Annu. Rev. Ecol. Evol. Syst., 42, 181-203, https://doi.org/10.1146/annurev-ecolsys-102209-144647, 2011.

Oki, T., and Kanae, S.: Global Hydrological Cycles and World Water Resources. Science, 313, 1068-1072, https://doi.org/10.1126/science.1128845, 2006.

Piao, S., Wang, X., Park, T., Chen, C., Lian, X., He, Y., Bjerke, J. W., Chen, A., Ciais, P., Tømmervik, H., Nemani, R. R., and R. B. Myneni.: Characteristics, drivers and feedbacks of global greening. Nature Reviews Earth & Environment, 1, 14-27, https://doi.org/10.1038/s43017-019-0001-x, 2020.

Piao, S., Friedlingstein, P., Ciais, P., Noblet-Ducoudre, N., Labat, D., and Zaehle, S.: Changes in climate and land use have a larger direct impact than rising CO_2 on global river runoff trends. Proc. Natl. Acad. Sci. 104, 15242-15247, https://doi.org/10.1073/pnas.0707213104, 2007.

Pinzon, J., and Tucker, C. A.: Non-Stationary 1981–2012 AVHRR NDVI3g Time Series. Remote Sens. 6, 6929, https://doi.org/10.3390/rs6086929, 2014.

Pregitzer, K. S. et al. Fine Root Architecture of Nine North American Trees. Ecol. Monogr., 72, 293-309, https://doi.org/10.1890/0012-9615(2002)072[0293:FRAONN]2.0.CO;2, 2002.

Porporato, A., Daly, E., and Rodriguez-Iturbe, I.: Soil Water Balance and Ecosystem Response to Climate Change. The Amer. Nat., 164, 625-632, https://doi.org/10.1086/424970, 2004.

Roderick, M. L., and Farquhar, G. D.: A simple framework for relating variations in runoff to variations in climatic conditions and catchment properties. Water Resour. Res. 47, W00G07, https://doi.org/10.1029/2010WR009826, 2011.

Roderick, M. L., Sun, F., Lim, W. H., and Farquhar, G. D.: A general framework for understanding the response of the water cycle to global warming over land and ocean. Hydrol. Earth Syst. Sci., 18, 1575-1589, https://doi.org/10.5194/hess-18-1575-2014, 2014.

Saxton, K. E., and Rawls, W. J.: Soil Water Characteristic Estimates by Texture and Organic Matter for Hydrologic Solutions. Soil Sci. Soc. Am J. 70, 1569-1578, https://doi.org/10.2136/sssaj2005.0117, 2006.

Shuttleworth, W. J., and Wallace, J. S.: Evaporation from sparse crops-an energy combination theory. Q. J. R. Meteorol. Soc. 111, 839-855, https://doi.org/10.1002/qj.49711146910, 1985.

Siebert, S., Doll, P., Hoogeveen, J., Faures, J. M., Frenken, K., and Feick, S.: Development and validation of the global map of irrigation areas. Hydrol. Earth Syst. Sci., 9, 535-547, https://doi.org/10.5194/hess-9-535-2005, 2005.

Swann, A. L. S., Hoffman, F. M., Koven, C. D., and Randerson, J. T.: Plant responses to increasing CO_2 reduce estimates of climate impacts on drought severity, Proc. Nati. Acad. Sci., 113, 10019-10024, https://doi.org/10.1073/pnas.1604581113, 2016.

Trancoso, R., Larsen, J.R., McVicar, T.R., Phinn, S.R., and McAlpine, C.A.: CO_2-vegetation feedbacks and other climate changes implicated in reducing base flow. Geophysical Research Letters, 44, 2310–2318, https://doi.org/10.1002/2017GL072759, 2017

Ukkola, A. M., Prentice, I. C., Keenan, T. F., van Dijk, A. I. J. M., Viney, N. R., Myneni, R. B., and Bi, J.: Reduced streamflow in water-stressed climates consistent with CO_2 effects on vegetation. Nature Clim. Change, 6, 75-78, https://doi.org/10.1038/nclimate2831, 2016.

Wei, Y. et al. The North American Carbon Program Multi-scale Synthesis and Terrestrial Model Intercomparison Project – Part 2: Environmental driver data. Geosci. Model Dev. 7, 2875-2893, https://doi.org/10.5194/gmd-7-2875-2014, 2014.

Wong, S. C., Cowan, I. R., and Farquhar, G. D.: Stomatal conductance correlates with photosynthetic capacity. Nature 282, 424-426, https://doi.org/10.1038/282424a0, 1979.

Yang, Y., Donohue, R. J., and McVicar, T. R.: Global estimation of effective plant rooting depth: Implications for hydrological modeling. Water Resour. Res., 52, 8260-8276, https://doi.org/10.1002/2016WR019392, 2016b.

Yang, Y., Donohue, R. J., McVicar, T. R., Roderick, M. L., and Beck, H. E.: Long-term CO_2 fertilization increases vegetation productivity and has little effect on hydrological partitioning in tropical rainforests. J. Geophys. Res. Biogeosci., 121, 2125-2140, https://doi.org/10.1002/2016JG003475, 2016a.

Yang, Y., Randall, R. J., McVicar, T. R. & Roderick, M. L. An analytical model for relating global terrestrial carbon assimilation with climate and surface conditions using a rate limitation framework. Geophys. Res. Lett., 42, 9825-9835, https://doi.org/10.1002/2015GL066835, 2015.

Yang, Y., Roderick, M. L., Zhang, S., McVicar, T. R., Donohue, R. J.: Hydrologic implications of vegetation response to elevated CO_2 in climate projections. Nature Climate Change, 9, 44-48, https://doi.org/10.1038/s41558-018-0361-0, 2019.

Zhang, C., Yang, Y., Yang, D., Wang, Z. R., Wu, X., Zhang, S. L., and Zhang, W. J.: Vegetation response to elevated CO_2 slows down the eastward movement of the 100th meridian. Geophys. Res. Lett., 47, e2020GL089681, https://doi.org/10.1029/2020GL089681, 2020a.

Zhang, C., Yang, Y., Yang, D., and Wu, X.: Multidimensional assessment of global dryland changes under future warming in climate projections. J. Hydrol., 125618, https://doi.org/10.1016/j.jhydrol.2020.125618, 2020b.

Zhang, Y. Q., Viney, N., Frost, A., Oke, A., Brooks, M., Chen, Y., Campbell, N. Collation of Australian modeller's streamflow dataset for 780 unregulated Australian catchments. CSIRO, Canberra, 2013.

Zhu, Z., Piao, S., Myneni, R. B., Huang, M., Zeng, Z., Canadell, J. G., Ciais, P., Sitch, S., Friedlingstein, P., Arneth, A., Cao, C., Cheng, L., Kato, E., Koven, C., Li, Y., Lian, X., Liu, Y., Liu, R., Mao, J., Pan, Y., Peng, S., Peñuelas, J., Poulter, B., Pugh, T., Stocker, B. D., Viovy, N., Wang, X., Wang, Y., Xiao, Z., Yang, H., Zaehle, S., Zeng N.: Greening of the earth and its drivers, Nat. Clim. Change, 6, 791–795, https://doi.org/10.1038/nclimate3004, 2016.

Zhu, Z. et al.: Global Data Sets of Vegetation Leaf Area Index (LAI)3g and Fraction of Photosynthetically Active Radiation (FPAR)3g Derived from Global Inventory Modeling and Mapping Studies (GIMMS) Normalized Difference Vegetation Index (NDVI3g) for the Period 1981 to 2011. Remote Sens. 5, 22, https://doi.org/10.3390/rs5020927, 2013.

https://doi.org/10.5194/hess-2020-548
Preprint. Discussion started: 14 December 2020


Hydrology and Earth System Sciences
Discussions

List of Figures

Figure 1 Spatial distributions of (a) resource availability index and (b) climate aridity zones for 1982-2010.

Figure 2 Location of global catchments. The grey dots show the locations of the original 21,856 catchments, and red dots are the 2,268 catchments that pass the selection criteria and are used herein.

Figure 3 Validation of estimated *Q* at catchments. a, Model performance in predicting mean annual *Q* in 2,268 catchments. Red dots in global maps show the location of catchments. **b**, Model performance in predicting *Q* trend in 2,268 catchments during 1982-2010. **c**, same as a, but for each resource availability category. **d**, same as b, but for each resource availability category. The legend from **c** applies to **d.** In **c** and **d**, the upper / lower box edges represent the quantile divisions, the inner horizontal line is the median, the dots indicate the mean value, and the dashed line represent the 5% and 95% percentiles.

Figure 4 Relative changes in *L* and Z_e caused by eCO_2. **a**, Spatial distribution of relative change in *L* induced by eCO_2 during 1982-2010. **b**, Same as a, but for each but for each resource availability category. **c**, Validation of predicted *L* change against *in situ* measurement during six Free Air CO_2 Enrichment (FACE) Experiments. Note that only FACE sites with undisturbed vegetation are used (see Donohue et al., 2017 for selection of undisturbed FACE sites). **d**, Spatial distribution of relative change in Z_e induced by eCO_2 during 1982-2010. **e**, Same as d, but for each resource availability category. In **b** and **e**, the upper / lower box edges represent the quantile divisions, the inner horizontal line is the median, the dots indicate the mean value, and the dashed line represent the 1% and 99% percentiles.

Figure 5 Relative *Q* change induced by eCO_2 during 1982-2010 at catchments. a, Relative change in *Q* induced by eCO_2 as a function of resource availability index for all 2,268 catchments. The red line is the best linear fit. **b**, Same as a, but for each resource availability category. In **b**, the upper / lower box edges represent the quantile divisions, the inner horizontal line is the median, the dots indicate the mean value, and the dashed line represent the 1% and 99% percentiles.

Figure 6 Attribution of changes in *Q* between 1982-1985 and 2006-2010 at catchments. a, Attribution of changes in *Q* between 1982-1985 and 2006-2010 for all 2,268 catchments. **b-f**, Attribution of changes in *Q* between 1982-1985 and 2006-2010 for catchments within each resource availability category. Error bars indicate one tenth of standard deviation of each response among catchments. For each subplot the values above the observed d*Q* and modelled d*Q* columns represent the mean value and have units of mm yr^{-1}. Whereas the values in parenthesis of the four columns to the right of the vertical grey dashed line represent the percent contribution each factor induced in the observed d*Q* change. The number of catchments in each group is provided on Figure 3(d).

https://doi.org/10.5194/hess-2020-548
Preprint. Discussion started: 14 December 2020


Hydrology and Earth System Sciences
Discussions

Figure 7 Sensitivity of *Q* to eCO_2 and its relative importance to *P* and E_P across the globe. a, Spatial distribution of *Q* sensitivity to eCO_2 (% change in *Q* per 1% change in C_a). **b**, Boxplot of *Q* sensitivity to eCO_2 for each resource availability category. **c**, Relative importance of eCO_2 on *Q* compared to changes in *P* on *Q* (% change in *Q* per 1% change in C_a compared to % change in *Q* per 1% change in *P*). **d**, Boxplot of the relative importance of eCO_2 on *Q* compared to changes in *P* on *Q* for each resource availability category. **e**, Relative importance of eCO_2 on *Q* compared to changes in E_P on *Q* (% change in *Q* per 1% change in C_a compared to % change in *Q* per 1% change in E_P). **f**, Boxplot of the relative importance of eCO_2 on *Q* compared to changes in E_P on *Q* for each resource availability category. In **b**, **d** and **f** the upper / lower box edges represent the quantile divisions, the inner horizontal line is the median, the dots indicate the mean value, and the dashed line represent the 1% and 99% percentiles.

https://doi.org/10.5194/hess-2020-548
Preprint. Discussion started: 14 December 2020

Hydrology and Earth System Sciences
Discussions

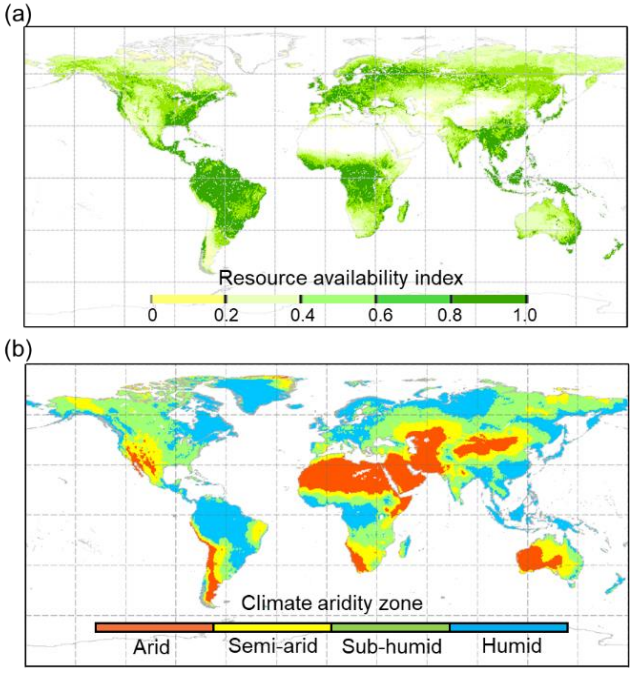

Figure 1 Spatial distributions of (a) resource availability index and (b) climate aridity zones for 1982-2010.

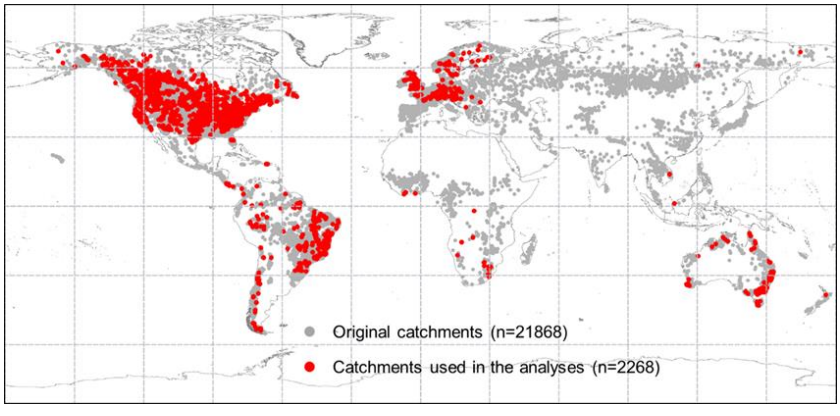

555

Figure 2 Location of global catchments. The grey dots show the locations of the original 21,856 catchments, and red dots are the 2,268 catchments that pass the selection criteria and are used herein.

https://doi.org/10.5194/hess-2020-548
Preprint. Discussion started: 14 December 2020

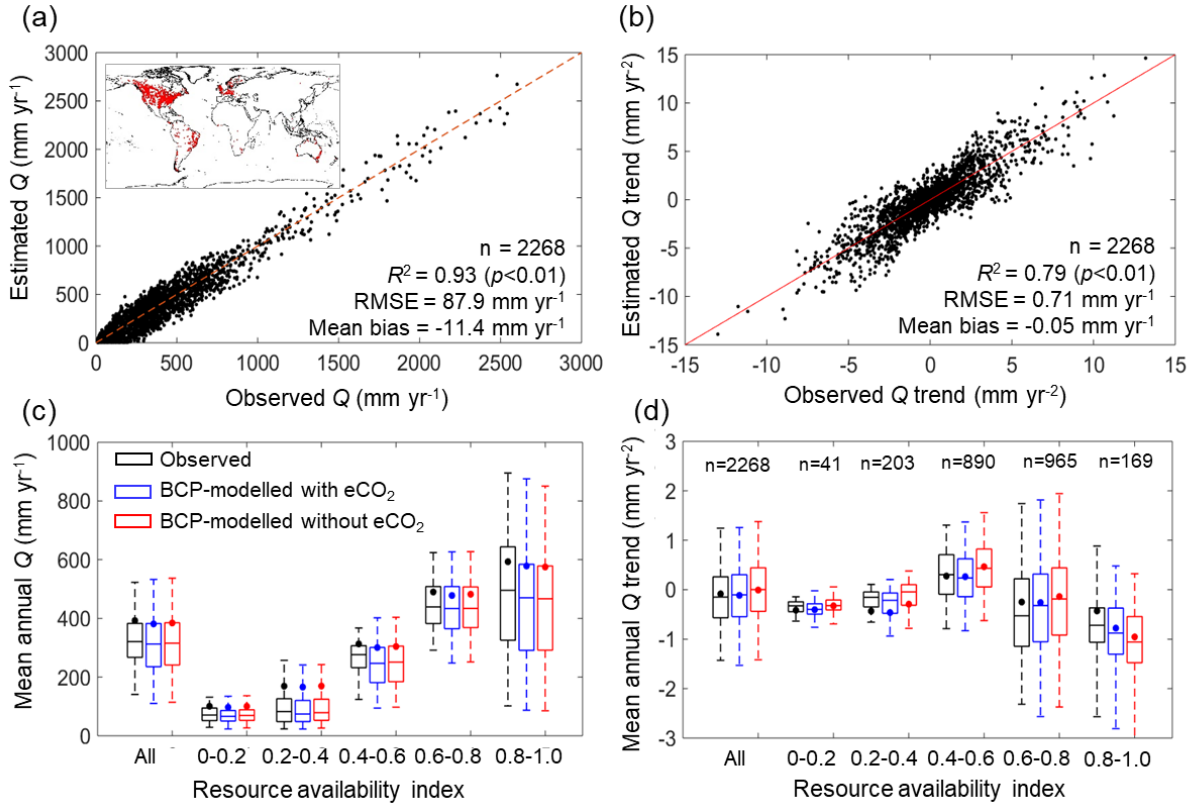

Figure 3 Validation of estimated *Q* at catchments. a, Model performance in predicting mean annual *Q* in 2,268 catchments. Red dots in global maps show the location of catchments. **b**, Model performance in predicting *Q* trend in 2,268 catchments during 1982-2010. **c**, same as a, but for each resource availability category. **d**, same as b, but for each resource availability category. The legend from **c** applies to **d.** In **c** and **d**, the upper / lower box edges represent the quantile divisions, the inner horizontal line is the median, the dots indicate the mean value, and the dashed line represent the 5% and 95% percentiles.

https://doi.org/10.5194/hess-2020-548
Preprint. Discussion started: 14 December 2020

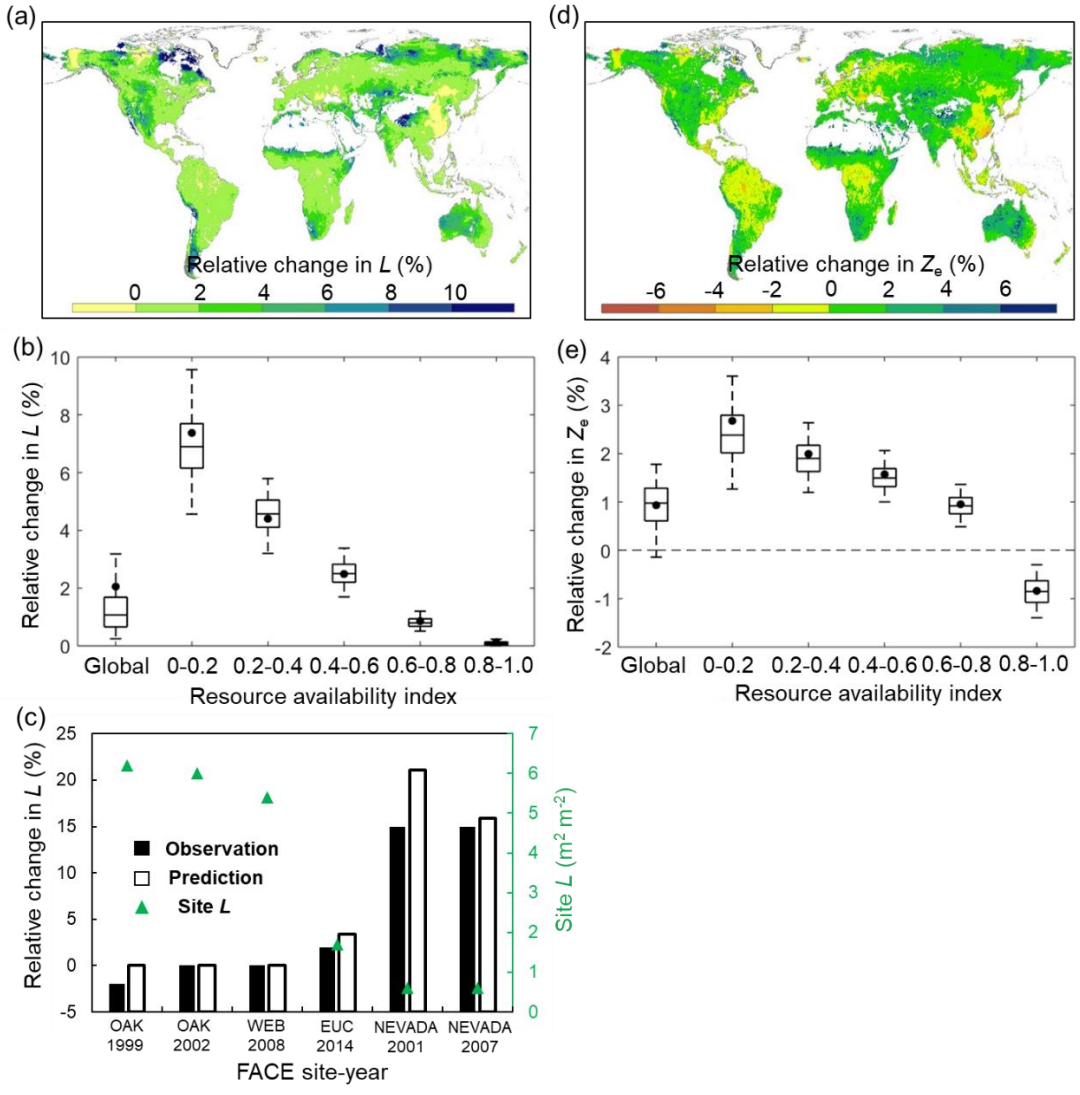

Figure 4 Relative changes in L and Z_e caused by eCO_2. **a**, Spatial distribution of relative change in L induced by eCO_2 during 1982-2010. **b**, Same as a, but for each but for each resource availability category. **c**, Validation of predicted L change against *in situ* measurement during six Free Air CO_2 Enrichment (FACE) Experiments. Note that only FACE sites with undisturbed vegetation are used (see Donohue et al., 2017 for selection of undisturbed FACE sites). **d**, Spatial distribution of relative change in Z_e induced by eCO_2 during 1982-2010. **e**, Same as d, but for each resource availability category. In **b** and **e**, the upper / lower box edges represent the quantile divisions, the inner horizontal line is the median, the dots indicate the mean value, and the dashed line represent the 1% and 99% percentiles.

https://doi.org/10.5194/hess-2020-548
Preprint. Discussion started: 14 December 2020

Hydrology and Earth System Sciences
Discussions

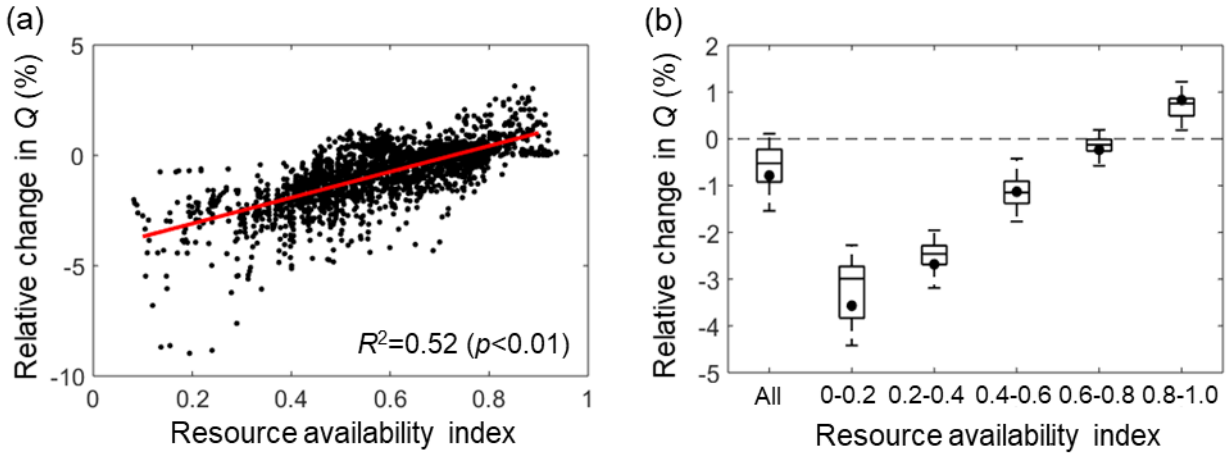

Figure 5 Relative *Q* change induced by eCO_2 during 1982-2010 at catchments. a, Relative change in *Q* induced by eCO_2 as a function of resource availability index for all 2,268 catchments. The red line is the best linear fit. **b**, Same as a, but for each resource availability category. In **b**, the upper / lower box edges represent the quantile divisions, the inner horizontal line is the median, the dots indicate the mean value, and the dashed line represent the 1% and 99% percentiles.

https://doi.org/10.5194/hess-2020-548
Preprint. Discussion started: 14 December 2020

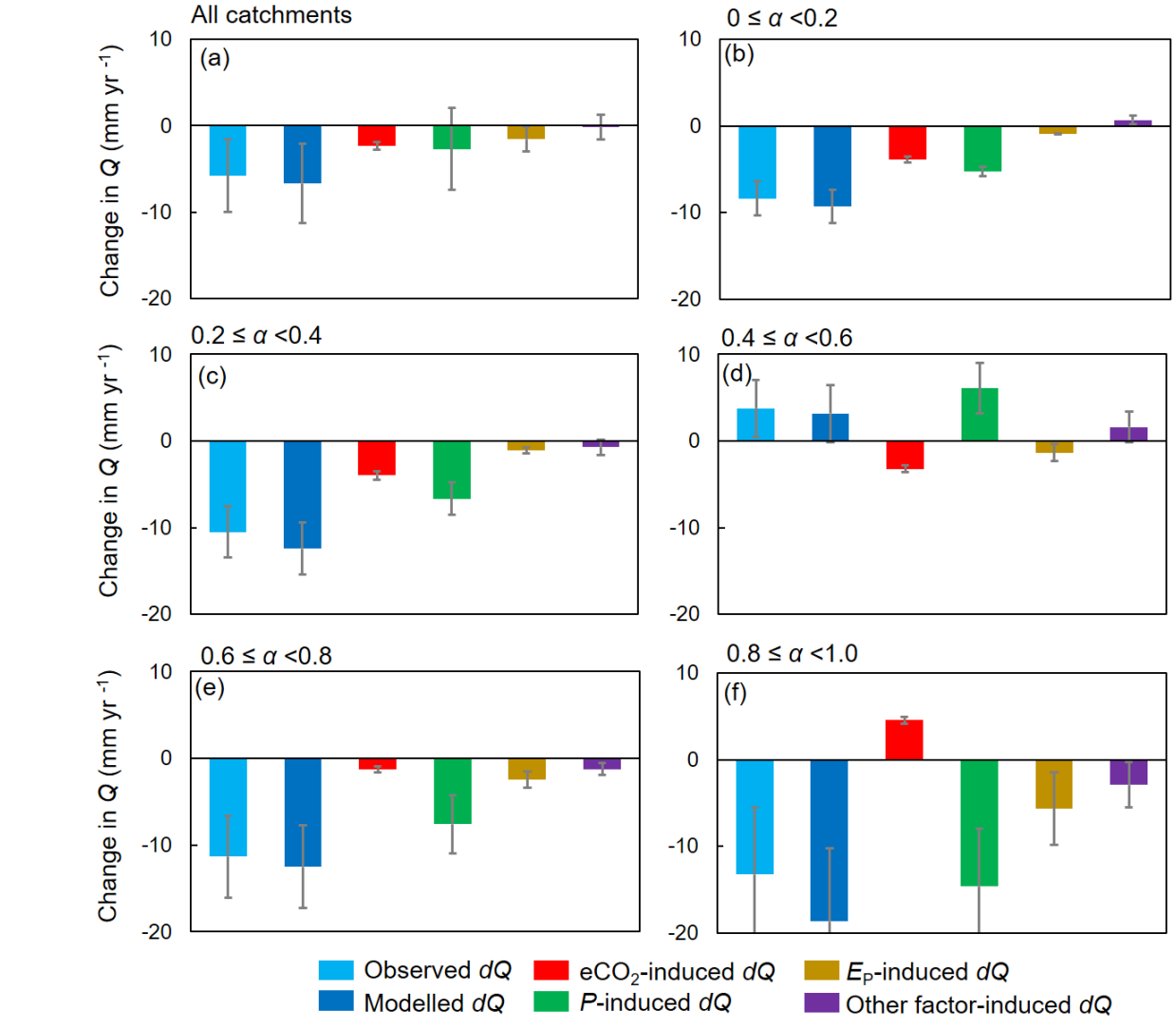

Figure 6 Attribution of changes in *Q* between 1982-1985 and 2006-2010 at catchments. a, Attribution of changes in *Q* between 1982-1985 and 2006-2010 for all 2,268 catchments. **b-f**, Attribution of changes in *Q* between 1982-1985 and 2006-2010 for catchments within each resource availability category. Error bars indicate one tenth of standard deviation of each response among catchments. For each subplot the values above the observed d*Q* and modelled d*Q* columns represent the mean value and have units of mm yr^{-1}. Whereas the values in parenthesis of the four columns to the right of the vertical grey dashed line represent the percent contribution each factor induced in the observed d*Q* change. The number of catchments in each group is provided on Figure 3(d).

https://doi.org/10.5194/hess-2020-548
Preprint. Discussion started: 14 December 2020

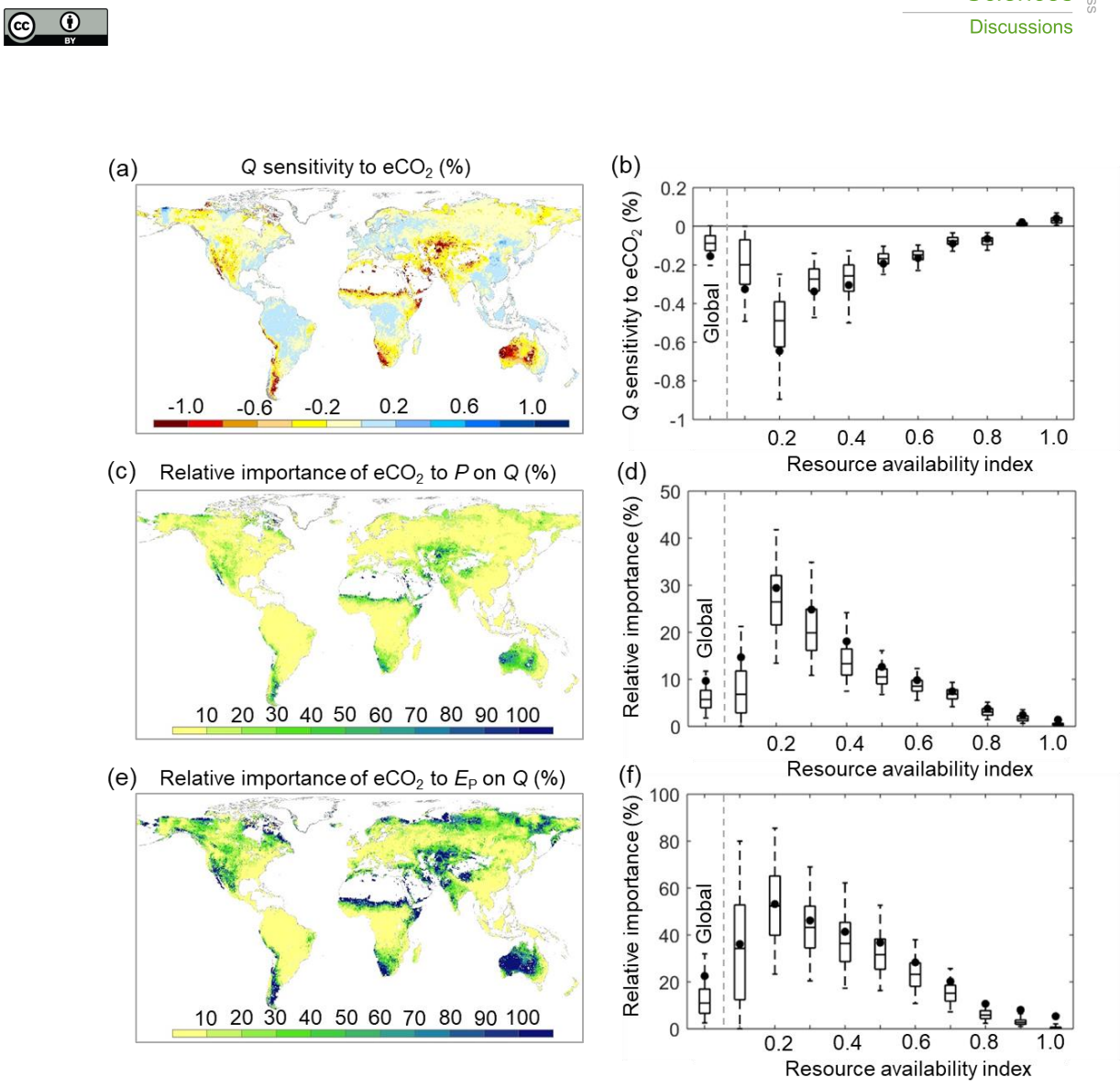

Figure 7 Sensitivity of *Q* to eCO_2 and its relative importance to *P* and E_P across the globe. a, Spatial distribution of *Q* sensitivity to eCO_2 (% change in *Q* per 1% change in C_a). **b**, Boxplot of *Q* sensitivity to eCO_2 for each resource availability category. **c**, Relative importance of eCO_2 on *Q* compared to changes in *P* on *Q* (% change in *Q* per 1% change in C_a compared to % change in *Q* per 1% change in *P*). **d**, Boxplot of the relative importance of eCO_2 on *Q* compared to changes in *P* on *Q* for each resource availability category. **e**, Relative importance of eCO_2 on *Q* compared to changes in E_P on *Q* (% change in *Q* per 1% change in C_a compared to % change in *Q* per 1% change in E_P). **f**, Boxplot of the relative importance of eCO_2 on *Q* compared to changes in E_P on *Q* for each resource availability category. In **b**, **d** and **f** the upper / lower box edges represent the quantile divisions, the inner horizontal line is the median, the dots indicate the mean value, and the dashed line represent the 1% and 99% percentiles.